THE JOURNAL OF PHYSICAL CHEMISTRY C

Article

pubs.acs.org/JPCC

Electron Transfer as a Probe of the Permeability of Organic Monolayers on the Surfaces of Colloidal PbS Quantum Dots

Kathryn E. Knowles, Mario Tagliazucchi, Michał Malicki, Nathaniel K. Swenson, and Emily A. Weiss*

Department of Chemistry, Northwestern University, 2145 Sheridan Road, Evanston, Illinois 60208, United States

Supporting Information

ABSTRACT: Transient absorption measurements on both the picosecond and microsecond time scales reveal that the efficiencies with which a series of alkyl-substituted *p*-benzoquinone (s-BQ) molecules participate in static and collisional photoinduced electron transfer (PET) with colloidal PbS quantum dots (QDs) in dichloromethane solution depend on both the size and shape of the s-BQ molecule. The efficiencies of both static and collisional PET are limited by the presence of the oleate ligand shell on the surface of the QDs and decrease with an increase in molecular volume, V_Q, of the s-BQ, in general; however, the substitution patterns on the BQ ring that facilitate static PET are not the same patterns that facilitate collisional PET. A model for the dependence of the collisional quenching efficiency on V_Q allows quantitative characterization of both the permeability and average thickness of the oleate ligand shell of the QDs in a dichloromethane solution.

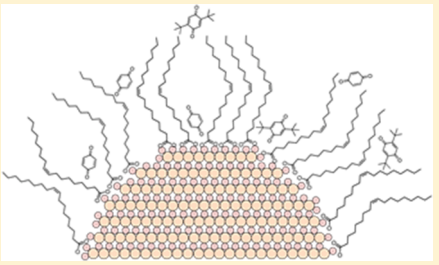

INTRODUCTION

This paper describes the influence of the size and shape of alkyl-substituted benzoquinone (s-BQ) acceptors on the efficiency with which they participate in static and collisional photoinduced electron transfer (PET) with oleate-coated PbS quantum dots (QDs) in a dichloromethane solution. Efficient extraction of photogenerated charge carriers from colloidal semiconductor QDs is essential to their application as photovoltaically and photocatalytically active materials.[1] The organic ligand shell that electronically passivates[2−4] and solubilizes[5] colloidal QDs also presents a physical barrier that impedes a molecular redox partner's approach to the QD surface and limits the number of available sites per QD for its adsorption.[6−9] The ligand shell therefore acts as a semipermeable self-assembled monolayer (SAM), the properties of which are traditionally investigated through the voltammetric behavior of SAM-coated planar or nanoparticulate metal substrates in the presence of electroactive molecular species.[10−16] Many careful studies, most often on SAMs of alkylthiols or disulfides on planar gold, have mapped the electrical current produced through heterogeneous charge transfer from the conductive substrate to a molecular probe to intra- and intermolecular structural characteristics of the SAM, including the length and saturation of alkyl chains, the charge of the chain's terminal group, and the density of pinholes, "thin" regions, and adventitious adsorbates.[12,14−21]

Cooperative effects among alkyl ligands that dictate the degree of structural ordering in planar monolayers play a qualitatively similar role for SAMs on nanoparticles,[21−23] but the high curvature of nanoparticle surfaces, and the presence of facets, edges, and vertices, also influence the organization and density of molecules on these surfaces.[9,17,23−27] The relationship between the structure of an organic adlayer on a nanoparticle and the nanoparticle's redox activity therefore is not directly analogous to that relationship for a planar surface. Furthermore, it is necessary to characterize this relationship for each type of nanoparticle−ligand system: the intermolecular order of an organic adlayer on a metal nanoparticle is inhibited primarily by the curvature of the nanoparticle surface, while the disorder of an adlayer on a semiconductor QD is amplified by structural disorder of the underlying inorganic core.[26]

Murray and co-workers studied thiolate layers on gold nanoparticles by cyclic voltammetry (CV) measurements in which they observed double-layer charging behavior analogous to the charging of a capacitor.[28] Semiconductor QDs (at least those with the most common organic adlayers), however, tend to undergo irreversible surface redox reactions, and often precipitate from solution, under applied potentials; this behavior makes it extremely difficult to obtain reproducible CV measurements of QDs in solution-phase equilibrium with their native ligands. Here we show that time-resolved optical studies of photoinduced charge transfer between colloidal QDs and molecules, during which the QDs are stable to flocculation and show reproducible behavior over hours or days, are useful for defining the pathways by which molecules permeate the ligand shell of the particle.

We have shown that the ability of a molecular redox partner to adsorb to the inorganic surface of a QD, where it can participate in photoinduced charge transfer on the single-picosecond time scale, depends on the density and permeability of the native ligand shell,[6,7] and that these properties are sensitive to the absolute concentration of the QDs[6] and the

Received: July 1, 2013
Revised: July 9, 2013

dx.doi.org/10.1021/jp406485y | J. Phys. Chem. C XXXX, XXX, XXX−XXX

binding headgroup of the native ligands.[7] For example, we observed that diluting solutions containing oleate-coated CdS QDs and viologen electron acceptors shifts the QD−oleate adsorption equilibrium toward more free native ligands and increases the number of available adsorption sites for the redox-active viologens by a factor of up to 30.[6] In another case, exchanging oleate surface ligands for decanethiolate ligands on PbS QDs decreased the average number of available adsorption sites per QD for aminoferrocene, a hole acceptor, from five to zero.[7] Once the "empty" sites on a QD surface are occupied by adsorbed redox-active molecules, some QD−molecule systems, specifically those for which the rate of excitonic decay in the QD is slower than the average rate of collisions between QDs and freely diffusing redox-active molecules, also participate in collisionally gated photoinduced charge transfer processes on the microsecond time scale.[8] The diffusion-controlled bimolecular rate constants for these processes reflect the efficiency of the collisional quenching process, which depends on the ability of the redox-active molecule to approach the QD core with a donor−acceptor distance and geometry that permits charge transfer.

This previous work established that the organic adlayer of the QD affects the redox activity of the QD. Here, we take the first step toward purposefully designing organic adlayers to control this redox activity in specific ways by examining the rates of both static and collisionally gated photoinduced electron transfer processes as a function of the size and shape of the molecular acceptor. For this study, we used mixtures of oleate-coated PbS QDs and alkyl-substituted BQs in dichloromethane. We have shown previously that the long (1−3 μs)[29−32] excited state lifetime of PbS QDs and the small ($\sim 10^2$ M^{-1}) equilibrium constant for adsorption of *p*-benzoquinone (BQ) to oleate-coated PbS QDs allow this donor−acceptor pair to participate in both static and collisional PET.[8] As expected, the presence of oleate ligands on the surface of the QDs limits the overall efficiency of PET by impeding the approach of BQ to the inorganic core of the QD. We find here, as in previous electrochemical studies of planar SAMs,[10,15] that the ligand shell acts as a medium for molecular recognition, in that the ability of an electroactive probe to permeate the ligand shell is sensitive to both the size and shape of the probe. We describe the trend in collisional quenching efficiency with molecular volume, V_Q, with a model for the effect of V_Q on the change in free energy associated with transfer of s-BQ from a dichloromethane solution into the oleate ligand shell. This model yields parameters that provide a quantitative measure of the average thickness and permeability of the organic adlayer of the QDs.

EXPERIMENTAL METHODS

Synthesis of PbS QDs. We adapted our procedure for synthesizing PbS QDs from that of Hines and Scholes.[33] We deaerated a mixture of 2.0 mL of oleic acid (OA) and 18.0 mL of 1-octadecene (ODE) in a 50 mL three-neck round-bottom flask at room temperature by bubbling the mixture with nitrogen for 30 min. Addition of PbO (0.36 g) followed by heating to 150 °C with stirring under a N_2 flow for 30 min produced a clear and colorless solution that was then cooled to 110 °C. Injection of 0.17 mL of hexamethyldisilathiane dissolved in 8 mL of ODE caused the solution to change from colorless to orange to brown within 3 s. After 10 min, we cooled the reaction mixture to room temperature in an ice bath and washed the reaction mixture twice with 50 mL of methanol. Addition of acetone (3:1 by volume) followed by centrifugation at 5000 rpm for 5 min produced dark brown pellets that we redispersed in 10 mL of hexanes, and precipitated a second time by adding methanol (1:1 by volume). Centrifugation produced dark brown pellets that we washed three times with acetone, dried, and redispersed in a minimal amount of hexanes to form the stock solution of PbS QDs. This synthesis produced PbS QDs with a band-edge absorption maximum at 937 nm, which corresponds to a radius of 1.6 nm based on the size calibration curve of Cademartiri et al.[31,34]

Preparation of Solutions of PbS QDs and s-BQ for Transient Absorption Measurements. We purchased all of the s-BQ molecules shown in Figure 1A from Sigma-Aldrich and used them as received. We removed the solvent from a stock solution of PbS QDs in hexane by evaporation under reduced pressure, washed the resulting solid three times with methanol and three times with acetone, and then redispersed the QDs in CH_2Cl_2 to a concentration of 1.7×10^{-5} M, as determined by the ground state absorption spectrum.[34] We produced a series of PbS/s-BQ solutions by adding 2 mL of the stock PbS solution (in CH_2Cl_2) to appropriate volumes of a stock solution of s-BQ in CH_2Cl_2 and adding CH_2Cl_2 such that the final volume of each solution was 4 mL, the final concentration of QDs in each solution was 8.6×10^{-6} M, and the final concentration of s-BQ ranged from 1 to 12 mM. Transient absorption measurements on the solutions were performed within 6 h of their preparation. We did not observe any degradation of any of the solutions after exposure to laser excitation for up to 1 h, and both the ultrafast and microsecond TA measurements were reproducible over multiple scans.

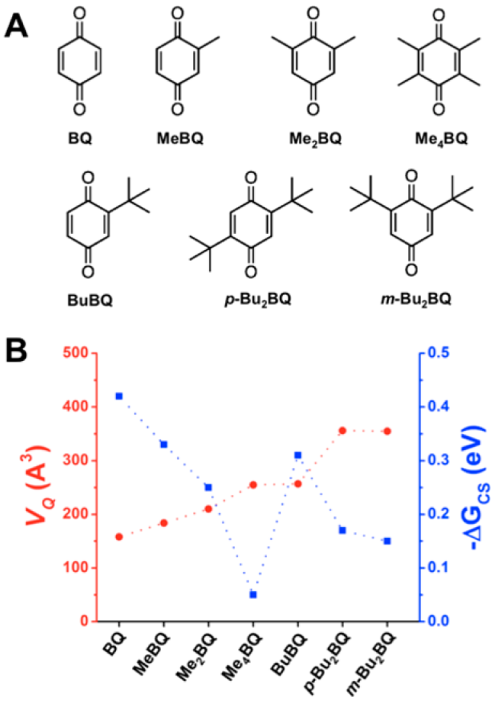

Figure 1. (A) Chemical structures of the s-BQ molecules used in this study. (B) Plot of the molecular volumes, V_Q (red circles), and the values of the driving force, $-\Delta G_{CS}$ (blue squares), for PET from the LUMO of a 1.6 nm PbS QD to the LUMO of each s-BQ. The dotted lines are guides for the eye.

Ultrafast Transient Absorption Spectroscopy. We split the 2.5 mJ output of a commercial amplified Ti-sapphire laser (Solstice, 1 kHz, 100 fs, Spectra Physics) and guided 95% to an

dx.doi.org/10.1021/jp406485y | J. Phys. Chem. C XXXX, XXX, XXX−XXX

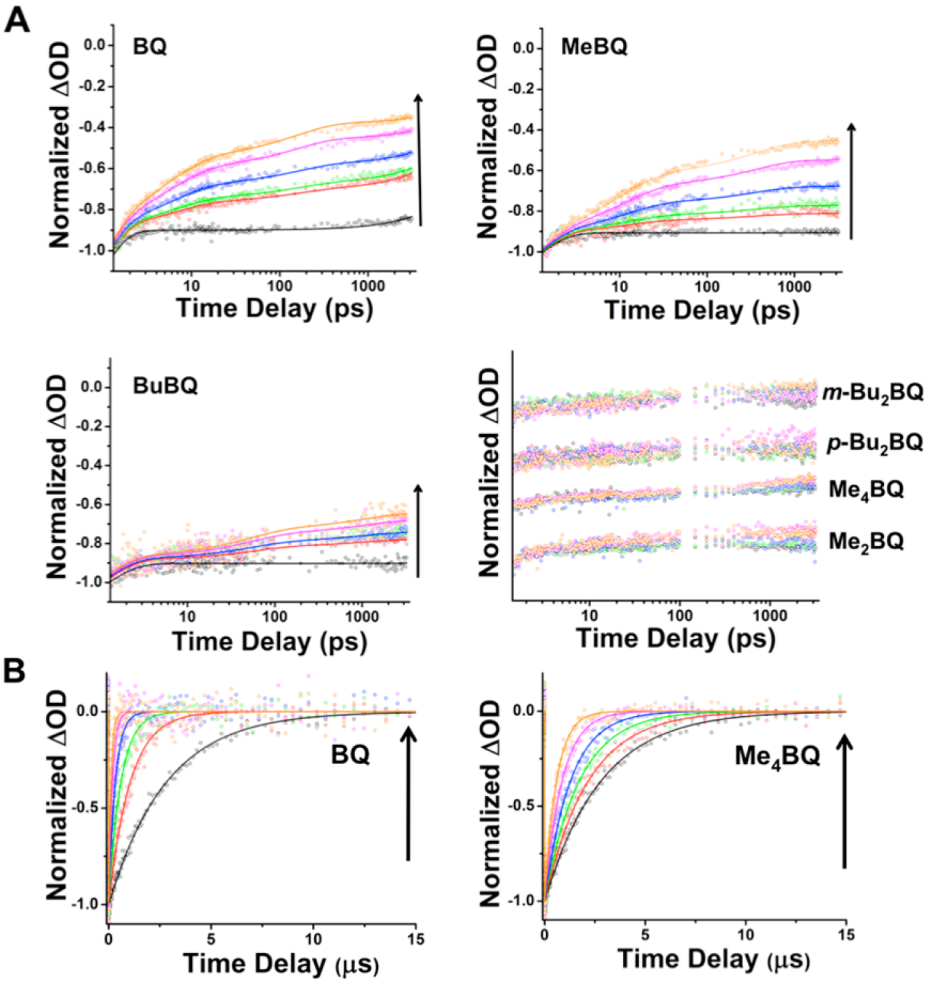

Figure 2. Kinetic traces at the ground state bleach feature on the picosecond (A) and microsecond (B) time scales of mixtures of 8.6×10^{-6} M PbS QDs with no added s-BQ molecules (black circles) and with concentrations of added s-BQ of 1, 2, 4, 8, and 12 mM (colored circles) in dichloromethane. (A) The black arrows on the picosecond plots for BQ, MeBQ, and BuBQ indicate increasing concentrations of added s-BQ, and the solid lines in these plots are global fits of the picosecond traces to eq 1. The picosecond traces for Me_2BQ, Me_4BQ, *p*-Bu_2BQ, and *m*-Bu_2BQ are offset vertically for the sake of clarity and show negligible changes in bleach dynamics with an increasing concentration of added s-BQ. (B) The solid lines represent fits of the microsecond traces to a single-exponential decay convoluted with an instrument response function. The microsecond kinetics for BQ and Me_4BQ shown here are representative of the microsecond kinetics obtained for the rest of the s-BQs, which are contained in the Supporting Information. Tables S3 and S4 of the Supporting Information contain values and uncertainties for all of the parameters used to fit the picosecond and microsecond time scale kinetic traces.

optical parametric amplifier (TOPAS-C, Light Conversion) used to produce the pump wavelength (915 nm) for sample excitation, and 5% to a commercial transient absorption (TA) spectrometer (HELIOS, Ultrafast Systems) for use as the probe for TA experiments with pump−probe delay times of up to 3200 ps. Within the spectrometer, a single filament broadband continuum of probe wavelengths from 900 to 1400 nm was generated in a 1.2 cm thick sapphire plate and then passed through a long-wave pass filter to isolate near-infrared wavelengths above 850 nm. The pump and probe were recombined at the sample, which was contained in a 2 mm quartz cuvette. The pump spot size was expanded to at least twice the size of the probe spot to compensate for any imperfections in translation stage alignment. The transmitted probe signal was collected into an optical fiber and dispersed onto an array detector. The output differential absorption spectrum (ΔA) was obtained through active background subtraction of the ground state spectrum by chopping the pump at 500 Hz. The pump light was depolarized to avoid the contribution of polarization dynamics in the collected data. Incident pump fluence was adjusted such that the ground state (GS) bleach dynamic for a solution of PbS QDs with no s-BQ exhibited no picosecond decay components associated with decay of multiexciton states. The solution was stirred with a magnetic stir bar to minimize local heating.

Microsecond Transient Absorption Spectroscopy. We used a commercial spectrometer (EOS, Ultrafast Systems) to collect TA spectra for pump−probe delay times from 0.5 ns to 25 μs. The excitation beam was generated by the same method and followed the same beam path as the excitation used for the ultrafast TA experiment described above. The proprietary EOS light source generates a supercontinuum (400−1700 nm) probe pulse by focusing a diode laser into a photonic crystal fiber. The repetition rate of the probe pulse is 2 kHz, which is twice the repetition rate of the pump pulse, and it is triggered in sync with the pump pulse. The pump−probe delay is electronically generated and measured by an electronic timer-counter-analyzer (Pendulum). After the probe pulse passes

dx.doi.org/10.1021/jp406485y | J. Phys. Chem. C XXXX, XXX, XXX−XXX

through an 850 nm long pass filter, a beam splitter sends half the probe pulse onto the sample, which was contained in a 2 mm quartz cuvette, and the other half of the probe pulse to a detector to act as a reference. The reference and sample beams are collected in optical fibers and dispersed onto array detectors. Dividing the signal from the sample beam by the reference signal allows us to divide out any fluctuations in the probe beam intensity during the experiment. The probe pulse was focused to a spot size of ~200 μm at the sample. To achieve a reasonable signal-to-noise ratio, the incident pump fluence was adjusted to generate an expectation value[35] ($\langle N \rangle$) of 1.0 in the first excitonic state of the QDs. The solution was stirred with a magnetic stir bar to minimize local heating.

RESULTS AND DISCUSSION

Photoinduced Electron Transfer from PbS QDs to s-BQ Molecules Occurs on the Picosecond and Microsecond Time Scales. Figure 1A shows the chemical structures of the s-BQ molecules studied here. Figure 1B shows a plot of the molecular volumes, V_Q, of the s-BQ series and the driving force, $-\Delta G_{CS}$, for electron transfer from the lowest unoccupied molecular orbital (LUMO) of a PbS QD with a radius of 1.6 nm to the LUMO of each s-BQ. We calculated $-\Delta G_{CS}$ from the reduction potentials of the s-BQ molecules, measured in CH_2Cl_2 with respect to ferrocene, and a literature value of the energy of the LUMO of 1.6 nm PbS QDs, measured by photoelectron emission spectroscopy in air (see the Supporting Information).[36] We define V_Q as the volume of the isosurface enclosing 99.7% of the total electron density of the s-BQ molecule and calculated it using density functional theory (DFT). The Supporting Information contains the details of this calculation, a discussion of two alternative methods for defining molecular volume, error bars for the molecular volume, and why we chose to use the total electron density to define molecular volume. Inspection of Figure 1B shows that photoinduced electron transfer from 1.6 nm PbS QDs to s-BQ is thermodynamically favorable for each s-BQ, by between 0.05 and 0.4 eV.

Figure 2 shows kinetic traces extracted from the ground state (GS) bleach feature in the transient absorption spectra of CH_2Cl_2 solutions of PbS QDs photoexcited into the lowest-energy excitonic state with and without added s-BQ. The Supporting Information contains a representative transient absorption spectrum of the PbS QDs used in this study. In the absence of added s-BQ molecules, the amplitude of the GS bleach feature does not decay detectably on the picosecond time scale (black traces in Figure 2A). Addition of BQ, MeBQ, or BuBQ to solutions of PbS QDs results in decay of the excitonic state of the PbS QDs on the picosecond time scale (Figure 2A), where the fraction of the excited state that decays increases with an increasing concentration of added s-BQ (each color in Figure 2 corresponds to a concentration of s-BQ between 1 and 12 mM). For a given concentration of added s-BQ, addition of BQ results in the greatest magnitude of excitonic decay on the picosecond time scale, followed by MeBQ and then BuBQ. Addition of any of the s-BQs with more than one substituent (Me_2BQ, Me_4BQ, *p*-Bu_2BQ, or *m*-Bu_2BQ) to solutions of PbS QDs does not accelerate excitonic decay in PbS QDs on the picosecond time scale (Figure 2A); that is, there is no discernible trend in the magnitude of the decay of the GS bleach with an increasing concentration of added s-BQ (see the Supporting Information).

Addition of any of the s-BQ molecules to the PbS QDs also increases the rate of excitonic decay on the microsecond time scale. Figure 2B shows two representative sets of kinetic traces of the recovery of the GS bleach feature on the microsecond time scale for mixtures of PbS QDs with and without added BQ and Me_4BQ. The Supporting Information contains kinetic traces for all of the s-BQs.

As in our previous work,[8] we attribute the acceleration of excitonic decay upon addition of s-BQ on both the picosecond and microsecond time scales to electron transfer from the lowest-energy state in the conduction band of photoexcited PbS QDs to the LUMO of a s-BQ molecule.

Only s-BQ Molecules with One or Fewer Substituents Participate in Static PET with PbS QDs. The rate of the PET process that occurs on the picosecond time scale is faster than the diffusion-limited rate of collisions between PbS QDs and s-BQ molecules ($k_{coll} < 10^9$ s^{-1}), given by the product of the diffusion-limited bimolecular rate constant, k_0, and the concentration of added s-BQ (see the Supporting Information). We therefore conclude that acceleration of excitonic decay on the picosecond time scale is due to static PET to s-BQ molecules that are already adsorbed to the surface of PbS QDs upon photoexcitation.

We use global fits of the sets of picosecond kinetic traces obtained for BQ, MeBQ, and BuBQ to eq 1 to determine the rate constants for charge separation, $k_{CS,int}$, and charge recombination, k_{CR}, associated with PET from PbS QDs to adsorbed BQ, MeBQ, and BuBQ.

$$\Delta OD(t) = -\{A_{CS}e^{-\langle N_{BQ,ads}\rangle}[\exp(\langle N_{BQ,ads}\rangle e^{-k_{CS,int}t}) - 1] + A_{CR}(1 - e^{-\langle N_{BQ,ads}\rangle})e^{-k_{CR}t} + e^{-\langle N_{BQ,ads}\rangle}e^{-t/\tau_{\mu s}} + A_{ph}e^{-k_{ph}t}\} \quad (1)$$

Equation 1 contains four components: (i) a Poisson-distributed charge separation component, with single donor−single acceptor rate constant $k_{CS,int}$, to account for the multiple charge separation pathways available to PbS QDs with more than one adsorbed s-BQ acceptor,[37,38] (ii) a single-exponential charge recombination component, with rate constant k_{CR}, (iii) a component with time constant $\tau_{\mu s}$, to account for the fraction of the GS bleach amplitude that decays on the microsecond time scale, and (iv) a component with rate constant k_{ph} and amplitude A_{ph}, to account for the small (~10% overall) contribution of a subpicosecond exciton decay process that likely originates from a phonon-mediated relaxation mechanism.[39] Parameters A_{CS} and A_{CR} account for the relative contributions of the electron and hole, respectively, to the total amplitude of the GS bleach, and $\langle N_{BQ,ads}\rangle$ is the average number of s-BQ molecules adsorbed per QD, given by the Poisson distribution. The derivation of eq 1 is described in detail elsewhere.[7,8]

In the global fit for each QD/s-BQ pair, the parameters A_{ph}, A_{CS}, A_{CR}, k_{CS}, k_{CR}, and k_{ph} are shared among all the kinetic traces corresponding to the set of added concentrations of s-BQ, $\tau_{\mu s}$ is fixed to the time constant obtained from a single-exponential fit to the corresponding kinetic trace for excitonic decay on the microsecond time scale, and $\langle N_{BQ,ads}\rangle$ is fixed to $-\ln(B/B_0)$, an expression derived from the Poisson distribution, where B/B_0 is the fraction of QDs with zero adsorbed s-BQ molecules.[37] We define B/B_0 as the ratio of the average bleach amplitude at delay times of 2500−3000 ps (after charge

dx.doi.org/10.1021/jp406485y | J. Phys. Chem. C XXXX, XXX, XXX−XXX

recombination) for samples of PbS QDs with (B) and without (B_0) added s-BQ.

Columns 1 and 2 of Table 1 contain the values of $k_{CS,int}$ and k_{CR} obtained from globally fitting the traces in Figure 2A to eq 1. The Supporting Information contains plots of the residuals for these fits. The rate constants of both charge separation and charge recombination between the QD and an adsorbed s-BQ decrease on going from BQ to MeBQ to BuBQ. Given the values of $-\Delta G_{CS}$ shown in Figure 1B and an estimated value of the reorganization energy associated with charge transfer from PbS QDs to s-BQ (λ) of 0.6 eV for all s-BQ molecules,[40] which is comparable to previously reported values of the reorganization energy associated with charge trapping processes in QDs,[41] the trends in $k_{CS,int}$ and k_{CR} are consistent with small (a factor of <2) differences in the magnitude of the electronic coupling between the donor (PbS QD) and acceptor (s-BQ) for BQ, MeBQ, and BuBQ, as calculated using the Marcus equation (see the Supporting Information).[42]

Table 1. Rate Constants and Numbers of Available Adsorption Sites for Static Charge Separation and Recombination between PbS QDs and Substituted BQs

s-BQ	$k_{CS,int}$ (s^{-1})	k_{CR} (s^{-1})	$\langle N_{sites}\rangle^a$
BQ	$(1.40 \pm 0.04) \times 10^{11}$	$(6.7 \pm 0.3) \times 10^{9}$	1.4 ± 0.1
MeBQ	$(7.5 \pm 0.2) \times 10^{10}$	$(2.9 \pm 0.2) \times 10^{9}$	1.7 ± 0.7
BuBQ	$(1.8 \pm 0.2) \times 10^{10}$	$(1.1 \pm 0.1) \times 10^{9}$	0.34 ± 0.05

$^a\langle N_{sites}\rangle = \theta_{max} \times 170$ is the average number of available adsorption sites per QD, as described in the text. The reported error in $\langle N_{sites}\rangle$ is propagated from the fit error in θ_{max}.

We used the values of $\langle N_{BQ,ads}\rangle = -\ln(B/B_0)$ for mixtures of PbS QDs with various concentrations of added BQ, MeBQ, and BuBQ to construct adsorption isotherms for these systems. We calculated the fractional surface coverage of s-BQ, θ, by dividing $\langle N_{BQ,ads}\rangle$ by the total number of adsorption sites on a PbS QD with a radius of 1.6 nm, which we estimate to be 170 (see the Supporting Information). Because $\langle N_{BQ,ads}\rangle < 1$ for all of the s-BQ/PbS QD mixtures studied here, we approximate the concentration of free s-BQ in solution to be the total concentration of added s-BQ, i.e., $[\text{s-BQ}]_{free} \approx [\text{s-BQ}]_{total}$. Figure 3 shows plots of θ versus $[\text{s-BQ}]_{free}$ for BQ, MeBQ, and BuBQ, and fits of these plots to the modified Langmuir isotherm given by eq 2,

$$\theta = \frac{\theta_{max} K_{ads} [\text{s-BQ}]_{free}}{1 + K_{ads} [\text{s-BQ}]_{free}} \quad (2)$$

where K_{ads} is the adsorption equilibrium constant and θ_{max} is the maximal fractional surface coverage that a s-BQ molecule can achieve, as limited by the oleate surface ligands. While we do not have enough data points to measure K_{ads} precisely enough to quantitatively distinguish the values of K_{ads} for BQ, MeBQ, and BuBQ from each other, we can estimate that the values of K_{ads} for all three of these s-BQ molecules are on the same order of magnitude ($\sim 10^2$ M^{-1}) as that for adsorption of ligands containing aromatic amine binding groups to the surfaces of PbS[7] or CdSe[9] QDs.

The three s-BQ molecules that participate in PET with PbS QDs on the ultrafast time scale, BQ, MeBQ, and BuBQ, have the three largest values of driving force for charge separation ($-\Delta G_{CS}$) among the series of s-BQ molecules shown in Figure 1. Therefore, one possible explanation for why Me_2BQ, Me_4BQ, p-Bu_2BQ, and m-Bu_2BQ do not participate in PET

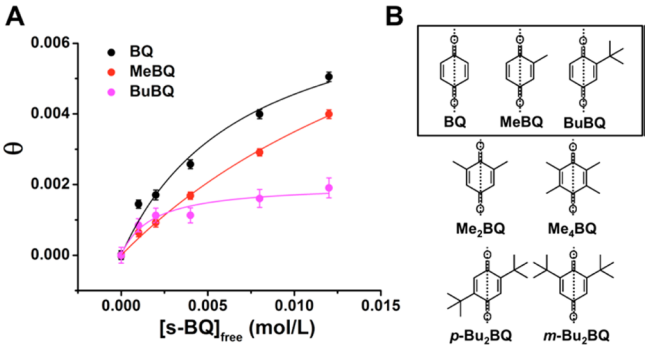

Figure 3. (A) Plots of fractional surface coverage of adsorbed s-BQ, θ, vs free s-BQ concentration in solution, $[\text{s-BQ}]_{free}$, for BQ, MeBQ, and BuBQ. The solid lines represent fits of these plots to the Langmuir equation (eq 2). The error bars are propagated from the standard deviation of the amplitudes of the GS bleach from 2500 to 3000 ps averaged to yield B/B_0. (B) Structures of s-BQ molecules with vertical dotted lines dividing the BQ ring in half along the axes of the carbonyl groups to illustrate the difference in the distribution of substituents between those s-BQs that participate in static PET (outlined by the black rectangle) and those s-BQs that do not participate in static PET.

with PbS QDs on the ultrafast time scale is that, even when they are adsorbed to the surface of the QD, PET from PbS to these BQs is too slow to observe on the ultrafast time scale because of their smaller values of $-\Delta G_{CS}$. A decrease in the driving force cannot, however, be responsible for the lack of observed dynamics for these molecules because, given the estimated reorganization energy of 0.6 eV, $k_{CS,int}$ for static PET from PbS to Me_4BQ (the s-BQ with the smallest driving force) is at least 4×10^8 s^{-1} ($\tau_{CS,int}$ = 2.5 ns), which is readily detectable in our experimental window for ultrafast TA. We therefore conclude that Me_2BQ, Me_4BQ, p-Bu_2BQ, and m-Bu_2BQ do not participate in static PET at all, which implies that they do not adsorb to the surfaces of the PbS QDs.

Figure 3A shows that BuBQ has a smaller θ_{max} than BQ or MeBQ for the same QDs. A smaller θ_{max} for BuBQ, the BQ with the bulkiest substituent of these three s-BQ molecules, indicates that there are fewer available adsorption sites per QD ($\langle N_{sites}\rangle = \theta_{max} \times 170$) for BuBQ than there are for BQ or MeBQ (Table 1). Simple size exclusion by the native ligand shell also explains why the two largest s-BQ molecules, p-Bu_2BQ and m-Bu_2BQ (Figure 1B), do not find adsorption sites on the QD surface. Consideration of only the molecular volume of the s-BQ in determining whether it will adsorb to the surface of a QD in a PET-active configuration does not explain, however, the absence of ultrafast PET in the QD/Me_2BQ and QD/Me_4BQ systems; these two molecules are smaller than or equal in size to BuBQ, which does participate in ultrafast PET. The one structural feature that consistently differentiates the s-BQs that adsorb to the QDs from those that do not is the number and distribution of the alkyl substituents on the BQ ring. Those s-BQs that have more than one alkyl substituent and, specifically, are substituted on both sides of an imaginary line dividing the BQ ring in half along the axes of the carbonyl groups do not participate in ultrafast PET (Figure 3B).

The Efficiency of Collisional PET from PbS QDs to s-BQ Depends on the Size and Shape of the s-BQ Molecule. Unlike the case for static PET, all of the s-BQs shown in Figure 1A participate in PET on the microsecond time scale. All of the microsecond kinetic traces fit to a single exponential multiplied by an instrument response function

dx.doi.org/10.1021/jp406485y | J. Phys. Chem. C XXXX, XXX, XXX−XXX

(IRF = 500 ps). Without added s-BQ (black traces in Figure 2B), the excited state of the PbS QD decays with a single time constant $\tau_{\mu s,0}$ of 2.8 μs, which is consistent with previous measurements on PbS QDs.[8,29,30]

Figure 4A shows plots of the ratio of the microsecond time constant for GS bleach recovery for a solution of PbS QDs with no added s-BQ ($\tau_{\mu s,0}$) to that for samples with added s-BQ ($\tau_{\mu s}$) versus the concentration of added s-BQ, [s-BQ], for each s-BQ. These plots are all linear and fit well to the linear Stern–Volmer equation (eq 3),[43] where k_q is the bimolecular quenching constant.

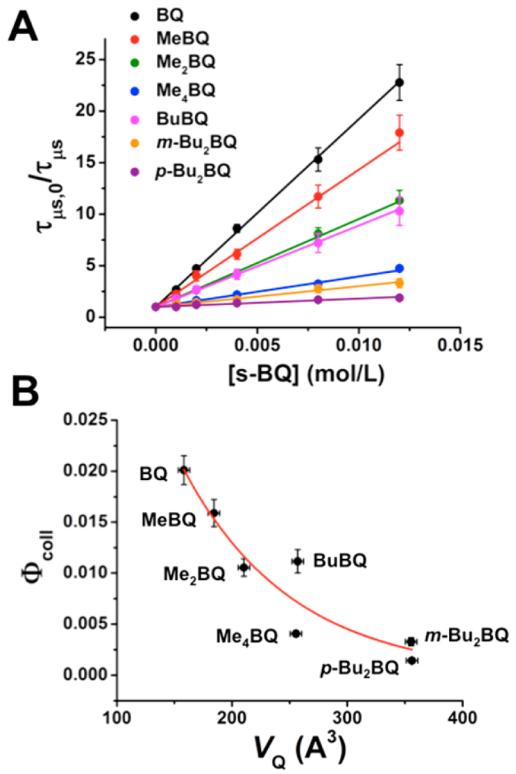

Figure 4. (A) Plots of the ratio of the microsecond time constant for ground state bleach recovery for a solution of PbS QDs with no added s-BQ ($\tau_{\mu s,0}$) to that for samples with added s-BQ ($\tau_{\mu s}$) vs the concentration of added s-BQ, [s-BQ], for each s-BQ. The error bars are propagated from the uncertainty in the values of $\tau_{\mu s,0}$ and $\tau_{\mu s}$ obtained from single-exponential fits of the microsecond kinetics (see the Supporting Information). The solid lines are fits of each data set to eq 3. (B) Plot of the collisional quenching efficiency, Φ_{coll}, calculated from eq 4 vs the molecular volume of s-BQ, V_Q. The vertical error bars are propagated from uncertainties in k_q and k_0, and the horizontal error bars are estimates of the uncertainty in the DFT calculation of V_Q (see the Supporting Information). The solid line is a fit of these data to eq 6.

$$\frac{\tau_{\mu s,0}}{\tau_{\mu s}} = 1 + k_q \tau_{\mu s,0}[\text{s-BQ}] \quad (3)$$

We assign the acceleration of excitonic decay on the microsecond time scale upon addition of s-BQ to collisional PET from photoexcited PbS QDs (with no adsorbed s-BQ) to freely diffusing s-BQ based on two observations: (i) the plots in Figure 4A fit well to the Stern–Volmer equation (eq 3), and (ii) the GS bleach decays to zero on the microsecond time scale with one decay component in all cases, that is, we do not observe a separate (concentration-independent) charge recombination component on the microsecond time scale.[8] These observations indicate that the rate of collisional PET from a PbS QD to a s-BQ molecule is limited by the ability of the s-BQ molecule to diffuse to a location near the inorganic core of the QD, where both the rates of charge separation and charge recombination are faster than the exciton recombination rate and the rate at which the s-BQ molecule diffuses away from this location.[8]

Table 2 contains the values of the slopes, $k_q\tau_{\mu s,0}$, obtained from linear fits of the plots in Figure 4A to eq 3 and the values of k_q for each s-BQ (calculated by dividing these slopes by a $\tau_{\mu s,0}$ of 2.8 μs). Table 2 also contains the values of the collisional quenching efficiency, Φ_{coll}, for each s-BQ calculated from eq 4, where k_0 is the diffusion-limited quenching constant given by eq 5,[43]

$$\Phi_{coll} = \frac{k_q}{k_0} \quad (4)$$

$$k_0 = \frac{4\pi N_A}{1000} R_C D_S \quad (5)$$

where R_C is the radius for a collision between an oleate-coated PbS QD and a freely diffusing s-BQ molecule, which we define to be the radius of the inorganic core of the PbS QD (1.6 nm), and D_S is the diffusion coefficient of the s-BQ molecule in dichloromethane. We measured D_S for each s-BQ by diffusion ordered (DOSY) ^{1}H NMR spectroscopy (see the Supporting Information). The Supporting Information describes the origin of the errors listed in Table 2.

Figure 4B contains a plot of Φ_{coll} versus the volume of the s-BQ molecules, V_Q. Inspection of Figure 4B and Table 2 reveals that the value of Φ_{coll} is $\leq$0.02 for all of the s-BQ molecules. The fact that the collisional quenching efficiencies are all much smaller than unity indicates that the ligand shell impedes the ability of the s-BQ molecules to approach the inorganic core of the QD.

The value of Φ_{coll} generally decreases with an increase in V_Q and generally increases with an increase in $|\Delta G_{CS}|$ (see the Supporting Information). We do not consider the correlation between Φ_{coll} and $-\Delta G_{CS}$ to be causal, however, because the

Table 2. Kinetic Parameters Describing Collisional PET from PbS QDs to Substituted BQs

s-BQ	$k_q\tau_{\mu s,0}$ (M^{-1})	k_q (M^{-1} s^{-1})	k_0 (M^{-1} s^{-1})	Φ_{coll}
BQ	1820 ± 40	(6.5 ± 0.2) × 10^8	(3.2 ± 0.2) × 10^{10}	0.020 ± 0.001
MeBQ	1330 ± 40	(4.7 ± 0.3) × 10^8	(3.0 ± 0.2) × 10^{10}	0.016 ± 0.001
Me_2BQ	850 ± 20	(3.0 ± 0.2) × 10^8	(2.9 ± 0.2) × 10^{10}	0.0105 ± 0.0009
Me_4BQ	300 ± 7	(1.06 ± 0.03) × 10^8	(2.6 ± 0.2) × 10^{10}	0.0041 ± 0.0003
BuBQ	790 ± 10	(2.7 ± 0.2) × 10^8	(2.5 ± 0.2) × 10^{10}	0.011 ± 0.001
m-Bu_2BQ	200 ± 14	(7.0 ± 0.7) × 10^7	(2.1 ± 0.1) × 10^{10}	0.0033 ± 0.0004
p-Bu_2BQ	80 ± 6	(3.0 ± 0.3) × 10^7	(2.1 ± 0.1) × 10^{10}	0.0014 ± 0.0002

dx.doi.org/10.1021/jp406485y | J. Phys. Chem. C XXXX, XXX, XXX–XXX

rate-limiting step for collisional PET is not charge separation at the QD surface, which depends on $-\Delta G_{CS}$, but rather diffusion of the s-BQ acceptor through the ligand shell to the surface of the QD, which does not depend on $-\Delta G_{CS}$. The observation that Φ_{coll} decreases with an increase in V_Q indicates that, again, the ligand shell is acting as a size-exclusion layer for approaching s-BQs. Zhang et al. observed a similar trend in the ability of electroactive substituted quinones of three different molecular sizes to exchange charge with planar gold substrates coated in mixed monolayers of mercaptopyrimidine (MP) and 1-dodecanethiol. They demonstrated a correlation between the size of the quinone that could permeate the monolayer and the average size of the MP domains ("thin regions") of the monolayer.[15]

We capture this size-exclusion behavior with a model that treats permeation through the ligand shell as the rate-limiting step for collisionally gated PET. This model divides the space surrounding the inorganic core of a PbS QD into two phases, an oleate ligand phase, L, and a dichloromethane solvent phase, S, in which the s-BQ molecules have different diffusion coefficients. D_S is the diffusion coefficient of a s-BQ molecule in the solvent phase, as measured by DOSY NMR, and D_L is the diffusion coefficient of a s-BQ molecule in the oleate ligand phase (see the Supporting Information for a diagram). The ability of a s-BQ molecule to permeate through the ligand phase depends on two parameters: (i) the change in free energy associated with transferring a s-BQ molecule from the solvent phase to the ligand phase, $\Delta G_{transfer}$, and (ii) D_L.[44,45] The border between the solvent and ligand phases is a virtual membrane that is permeable to s-BQ and solvent molecules, but not to oleate ligands; thus, we define $\Delta G_{transfer}$ as the product of the difference in osmotic pressure between the solvent and ligand phases and the volume of the s-BQ molecule.[46] This definition assumes that the primary contribution to the transfer energy is steric repulsion between the oleate ligands and s-BQ and leads to eq 6

$$\Phi_{coll} = \left(\frac{D_L}{D_S}\right)\left(\frac{R_L}{R_L - R_C}\right) \times \exp\left[\frac{V_Q}{V_S}\ln\left(1 - \frac{N_L V_L}{\frac{4}{3}\pi({R_L}^3 - {R_C}^3)}\right)\right] \quad (6)$$

where R_C is the radius of the QD core (1.6 nm), R_L is the radius of the QD core plus the thickness of the oleate ligand shell, V_S is the volume of a solvent molecule, V_L is the volume of an oleate ligand, and N_L is the number of oleate ligands bound per QD. The Supporting Information contains the derivation of eq 6.

We calculated V_S and V_L by the same DFT methodology we used to calculate V_Q, and we measured N_L by quantitative ^{1}H NMR spectroscopy (see the Supporting Information). These estimates leave two fitting parameters in eq 6, D_L/D_S and R_L, that we allow to float in our fit of the data in Figure 4B. This fit yields the following values: R_L = 2.9 nm, and D_L/D_S = 0.048. Because R_L represents the sum of the inorganic core radius (1.6 nm) and the thickness of the ligand shell, the value we obtain for R_L yields an average thickness for the oleate ligand shell of 1.3 nm. This thickness is less than the length of a fully extended oleate molecule (1.9 nm),[47] because of (i) the presence of *gauche* defects in the oleate chains,[25,26,48] (ii) the presence of gaps within the oleate ligand shell, or (iii) a combination of the two.

The parameter D_L/D_S provides a quantitative measurement of the permeability of the oleate ligand phase. Specifically, the D_L/D_S value of 0.048 indicates that the ligand shell slows the diffusion of all of the s-BQ molecules by a factor of 21 relative to diffusion in the solvent phase.

While eq 6 fits the general trend of a decreasing Φ_{coll} with an increasing V_Q, it is clear from Figure 4B that Φ_{coll} also depends on the shape of the s-BQ molecule. For instance, there are two pairs of s-BQ molecules that have the same volume but different values of Φ_{coll}. These pairs are BuBQ and Me_4BQ (V_Q = 250 Å^3) and *m*-Bu_2BQ and *p*-Bu_2BQ (V_Q = 350 Å^3). Within these two pairs of s-BQ molecules, the s-BQs with the larger collisional quenching efficiencies, BuBQ and *m*-Bu_2BQ, each contain one sterically unhindered oxygen atom with no proximal alkyl substituents. In contrast, both carbonyl oxygens in Me_4BQ and *p*-Bu_2BQ have at least one proximate alkyl substituent. These results indicate that, for s-BQ molecules with the same volume, the s-BQ with the least sterically hindered oxygen atoms has a larger collisional quenching efficiency.

CONCLUSIONS

Transient absorption measurements on the picosecond and microsecond time scales of solutions containing oleate-coated PbS QDs and various concentrations of s-BQ revealed that a combination of the size and shape of a s-BQ molecule determines the efficiency of both static and collisional PET from PbS QDs to the s-BQ. Each of a series of alkyl-substituted BQ molecules (Figure 1A) participates in collisional PET with oleate-coated PbS QDs (Figures 2B and 4A), but only s-BQ molecules with one or fewer substituents participate in static PET with PbS QDs (Figure 2A). Larger s-BQ molecules generally have fewer adsorption sites available on the surface of a PbS QD (Figure 3A) and do not permeate through the oleate ligand shell as easily as smaller s-BQ molecules (Figure 4B). Both the ability of a s-BQ to adsorb to the surface of a PbS QD (and participate in static PET) and its ability to permeate the oleate ligand shell (and participate in collisional PET) depend on the distribution of substituents on the BQ ring (i.e., its shape), but the two processes do not appear to have the same geometric requirements for the redox probe. This observation is not necessarily surprising if we imagine the ligand shell to have both "permanent" defects that serve as adsorption sites for the formation of static QD−s-BQ complexes and transient pathways (formed by conformational motion or temporary displacement of the native ligands) for diffusion of s-BQ molecules.

Our observation of collisional PET from PbS QDs to s-BQ molecules that do not participate in static PET demonstrates directly that a molecular redox partner does not have to be statically adsorbed to the surface of a QD to participate in photoinduced charge transfer with the QD. Removing the requirement for a surface binding group allows a greater synthetic flexibility in the design of molecular redox partners for colloidal QDs. Furthermore, this work demonstrates that the ability of a molecular redox partner to permeate the organic shell of a QD should be an important criterion in the design of components for QD-based photoelectrochemical systems. Equation 6 provides a parameter, D_L/D_S, that quantifies the permeability of the ligand shell of a QD in a specific solvent system for a given chemical structure of a redox probe. We hope to use this model to evaluate the molecular recognition

dx.doi.org/10.1021/jp406485y | J. Phys. Chem. C XXXX, XXX, XXX−XXX

properties of a variety of SAMs on colloidal quantum dots with the same specificity that has been achieved in planar systems.

■ ASSOCIATED CONTENT

Supporting Information

Details of the calculation of molecular volumes, DOSY NMR measurements, cyclic voltammetry of s-BQ molecules, characterization of PbS QDs, calculation of $-\Delta G_{CS}$, microsecond TA dynamics and time constants, residuals of fits of picosecond TA dynamics to eq 1, estimation of reorganization energy, error analysis, plot of Φ_{coll} versus $-\Delta G_{CS}$, and derivation of eq 6. This material is available free of charge via the Internet at http://pubs.acs.org.

■ AUTHOR INFORMATION

Corresponding Author

*E-mail: e-weiss@northwestern.edu.

Notes

The authors declare no competing financial interest.

■ ACKNOWLEDGMENTS

This work was supported primarily by a grant from the Air Force Office of Scientific Research (AFOSR) (FA9550-10-1-0220) through a Young Investigator Award to E.A.W. (experimental work) and as part of the Nonequilibrium Research Center, an Energy Frontier Research Center funded by the U.S. Department of Energy (DOE), Office of Science, Basic Energy Sciences (BES), under Award DE-SC0000989 (modeling). K.E.K. is supported by the Department of Energy Office of Science Graduate Fellowship Program (DOE SCGF), made possible in part by the American Recovery and Reinvestment Act of 2009, administered by ORISE-ORAU under Contract DE-AC0506OR23100.

■ REFERENCES

(1) Knowles, K. E.; Peterson, M. D.; McPhail, M. R.; Weiss, E. A. Exciton Dissociation within Quantum Dot-Organic Complexes: Mechanisms, Use as a Probe of Interfacial Structure, and Applications. *J. Phys. Chem. C* **2013**, *117*, 10229−10243.

(2) Klimov, V. I.; McBranch, D. W.; Leatherdale, C. A.; Bawendi, M. G. Electron and Hole Relaxation Pathways in Semiconductor Quantum Dots. *Phys. Rev. B* **1999**, *60*, 13740−13749.

(3) Knowles, K. E.; Tice, D. B.; McArthur, E. A.; Solomon, G. C.; Weiss, E. A. Chemical Control of the Photoluminescence of CdSe Quantum Dot-Organic Complexes with a Series of Para-Substituted Aniline Ligands. *J. Am. Chem. Soc.* **2010**, *132*, 1041−1050.

(4) Nose, K.; Fujita, H.; Omata, T.; Otsuka-Yao-Matsuo, S.; Nakamura, H.; Maeda, H. Chemical Role of Amines in the Colloidal Synthesis of CdSe Quantum Dots and Their Luminescence Properties. *J. Lumin.* **2007**, *126*, 21−26.

(5) Evans, C. M.; Cass, L. C.; Knowles, K. E.; Tice, D. B.; Chang, R. P. H.; Weiss, E. A. Review of the Synthesis and Properties of Colloidal Quantum Dots: The Evolving Role of Coordinating Surface Ligands. *J. Coord. Chem.* **2012**, *65*, 2391−2414.

(6) Morris-Cohen, A. J.; Vasilenko, V.; Amin, V. A.; Reuter, M. G.; Weiss, E. A. Model for Adsorption of Ligands to Colloidal Quantum Dots with Concentration-Dependent Surface Structure. *ACS Nano* **2012**, *6*, 557−565.

(7) Malicki, M.; Knowles, K. E.; Weiss, E. A. Gating of Hole Transfer from Photoexcited PbS Quantum Dots to Aminoferrocene by the Ligand Shell of the Dots. *Chem. Commun.* **2013**, *49*, 4400−4402.

(8) Knowles, K. E.; Malicki, M.; Weiss, E. A. Dual-Time Scale Photoinduced Electron Transfer from PbS Quantum Dots to a Molecular Acceptor. *J. Am. Chem. Soc.* **2012**, *134*, 12470−12473.

(9) Donakowski, M. D.; Godbe, J. M.; Sknepnek, R.; Knowles, K. E.; de la Cruz, M. O.; Weiss, E. A. A Quantitative Description of the Binding Equilibria of Para-Substituted Aniline Ligands and CdSe Quantum Dots. *J. Phys. Chem. C* **2010**, *114*, 22526−22534.

(10) Chailapakul, O.; Crooks, R. M. Interactions between Organized, Surface-Confined Monolayers and Liquid-Phase Probe Molecules. 4. Synthesis and Characterization of Nanoporous Molecular Assemblies: Mechanism of Probe Penetration. *Langmuir* **1995**, *11*, 1329−1340.

(11) Dolidze, T. D.; Rondinini, S.; Vertova, A.; Longhi, M.; Khoshtariya, D. E. Charge-Transfer Patterns for $[Ru(NH_3)_6]^{3+/2+}$ at Sam Modified Gold Electrodes: Impact of the Permeability of a Redox Probe. *Open Phys. Chem. J.* **2008**, *2*, 17−21.

(12) Campina, J. M.; Martins, A.; Silva, F. Selective Permeation of a Liquidlike Self-Assembled Monolayer of 11-Amino-1-Undecanethiol on Polycrystalline Gold by Highly Charged Electroactive Probes. *J. Phys. Chem. C* **2007**, *111*, 5351−5362.

(13) Bandyopadhyay, K.; Patil, V.; Sastry, M.; Vijayamohanan, K. Effect of Geometric Constraints on the Self-Assembled Monolayer Formation of Aromatic Disulfides on Polycrystalline Gold. *Langmuir* **1998**, *14*, 3808−3814.

(14) Subramanian, S.; Sampath, S. Enhanced Stability of Short- and Long-Chain Diselenide Self-Assembled Monolayers on Gold Probed by Electrochemistry, Spectroscopy, and Microscopy. *J. Colloid Interface Sci.* **2007**, *312*, 413−424.

(15) Zhang, H. L.; Chen, M.; Li, H. L. Study on Two-Component Matrix Formed by Coadsorption of Aromatic and Long Chain Mercaptans on Gold. *J. Phys. Chem. B* **2000**, *104*, 28−36.

(16) Ganesh, V.; Lakshminarayanan, V. Self-Assembled Monolayers of Alkanethiols on Gold Prepared in a Hexagonal Lyotropic Liquid Crystalline Phase of Triton X-100/Water System. *Langmuir* **2006**, *22*, 1561−1570.

(17) Laaksonen, T.; Pelliniemi, O.; Quinn, B. M. Ion Permeability of Sams on Nanoparticle Surfaces. *J. Am. Chem. Soc.* **2006**, *128*, 14341−14346.

(18) Twardowski, M.; Nuzzo, R. G. Phase Dependent Electrochemical Properties of Polar Self-Assembled Monolayers (Sams) Modified Via the Fusion of Mixed Phospholipid Vesicles. *Langmuir* **2004**, *20*, 175−180.

(19) Weiss, E. A.; Chiechi, R. C.; Kaufman, G. K.; Kriebel, J. K.; Li, Z. F.; Duati, M.; Rampi, M. A.; Whitesides, G. M. Influence of Defects on the Electrical Characteristics of Mercury-Drop Junctions: Self-Assembled Monolayers of N-Alkanethiolates on Rough and Smooth Silver. *J. Am. Chem. Soc.* **2007**, *129*, 4336−4349.

(20) Peng, Z. Q.; Dong, S. J. Formation of a Self-Assembled Monolayer of 2-Mercapto-3-N-octylthiophene on Gold. *Langmuir* **2001**, *17*, 4904−4909.

(21) Love, J. C.; Estroff, L. A.; Kriebel, J. K.; Nuzzo, R. G.; Whitesides, G. M. Self-Assembled Monolayers of Thiolates on Metals as a Form of Nanotechnology. *Chem. Rev.* **2005**, *105*, 1103−1169.

(22) Badia, A.; Lennox, R. B.; Reven, L. A Dynamic View of Self-Assembled Monolayers. *Acc. Chem. Res.* **2000**, *33*, 475−481.

(23) Templeton, A. C.; Wuelfing, M. P.; Murray, R. W. Monolayer Protected Cluster Molecules. *Acc. Chem. Res.* **2000**, *33*, 27−36.

(24) Peng, Z. Q.; Qu, X. H.; Dong, S. J. Immobilization of the Nanoparticle Monolayer onto Self-Assembled Monolayers by Combined Sterically Enhanced Hydrophobic and Electrophoretic Forces. *Langmuir* **2004**, *20*, 5−10.

(25) Meulenberg, R. W.; Bryan, S.; Yun, C. S.; Strouse, G. F. Effects of Alkylamine Chain Length on the Thermal Behavior of CdSe Quantum Dot Glassy Films. *J. Phys. Chem. B* **2002**, *106*, 7774−7780.

(26) Frederick, M. T.; Achtyl, J. L.; Knowles, K. E.; Weiss, E. A.; Geiger, F. M. Surface-Amplified Ligand Disorder in CdSe Quantum Dots Determined by Electron and Coherent Vibrational Spectroscopies. *J. Am. Chem. Soc.* **2011**, *133*, 7476−7481.

(27) Weeraman, C.; Yatawara, A. K.; Bordenyuk, A. N.; Benderskii, A. V. Effect of Nanoscale Geometry on Molecular Conformation: Vibrational Sum-Frequency Generation of Alkanethiols on Gold Nanoparticles. *J. Am. Chem. Soc.* **2006**, *128*, 14244−14245.

(28) Green, S. J.; Stokes, J. J.; Hostetler, M. J.; Pietron, J.; Murray, R. W. Three-Dimensional Monolayers: Nanometer-Sized Electrodes of Alkanethiolate-Stabilized Gold Cluster Molecules. *J. Phys. Chem. B* **1997**, *101*, 2663−2668.
(29) Gaponenko, M. S.; Lutich, A. A.; Tolstik, N. A.; Onushchenko, A. A.; Malyarevich, A. M.; Petrov, E. P.; Yumashev, K. V. Temperature-Dependent Photoluminescence of PbS Quantum Dots in Glass: Evidence of Exciton State Splitting and Carrier Trapping. *Phys. Rev. B* **2010**, *82*, 125320.
(30) Clark, S. W.; Harbold, J. M.; Wise, F. W. Resonant Energy Transfer in PbS Quantum Dots. *J. Phys. Chem. C* **2007**, *111*, 7302−7305.
(31) Warner, J. H.; Thomsen, E.; Watt, A. R.; Heckenberg, N. R.; Rubinsztein-Dunlop, H. Time-Resolved Photoluminescence Spectroscopy of Ligand-Capped PbS Nanocrystals. *Nanotechnology* **2005**, *16*, 175−179.
(32) Cademartiri, L.; Bertolotti, J.; Sapienza, R.; Wiersma, D. S.; von Freymann, G.; Ozin, G. A. Multigram Scale, Solventless, and Diffusion-Controlled Route to Highly Monodisperse PbS Nanocrystals. *J. Phys. Chem. B* **2006**, *110*, 671−673.
(33) Hines, M. A.; Scholes, G. D. Colloidal PbS Nanocrystals with Size-Tunable near-Infrared Emission: Observation of Post-Synthesis Self-Narrowing of the Particle Size Distribution. *Adv. Mater.* **2003**, *15*, 1844−1849.
(34) Cademartiri, L.; Montanari, E.; Calestani, G.; Migliori, A.; Guagliardi, A.; Ozin, G. A. Size-Dependent Extinction Coefficients of PbS Quantum Dots. *J. Am. Chem. Soc.* **2006**, *128*, 10337−10346.
(35) McArthur, E. A.; Morris-Cohen, A. J.; Knowles, K. E.; Weiss, E. A. Charge Carrier Resolved Relaxation of the First Excitonic State in CdSe Quantum Dots Probed with near-Infrared Transient Absorption Spectroscopy. *J. Phys. Chem. B* **2010**, *114*, 14514−14520.
(36) Jasieniak, J.; Califano, M.; Watkins, S. E. Size-Dependent Valence and Conduction Band-Edge Energies of Semiconductor Nanocrystals. *ACS Nano* **2011**, *5*, 5888−5902.
(37) Morris-Cohen, A. J.; Frederick, M. T.; Cass, L. C.; Weiss, E. A. Simultaneous Determination of the Adsorption Constant and the Photoinduced Electron Transfer Rate for a CdS Quantum Dot-Viologen Complex. *J. Am. Chem. Soc.* **2011**, *133*, 10146−10154.
(38) Sadhu, S.; Tachiya, M.; Patra, A. A Stochastic Model for Energy Transfer from CdS Quantum Dots/Rods (Donors) to Nile Red Dye (Acceptors). *J. Phys. Chem. C* **2009**, *113*, 19488−19492.
(39) Krauss, T. D.; Wise, F. W. Coherent Acoustic Phonons in a Semiconductor Quantum Dot. *Phys. Rev. Lett.* **1997**, *79*, 5102−5105.
(40) Marcus, R. A. On Theory of Electron-Transfer Reactions. 6. Unified Treatment for Homogeneous and Electrode Reactions. *J. Chem. Phys.* **1965**, *43*, 679−701.
(41) Jones, M.; Lo, S. S.; Scholes, G. D. Quantitative Modeling of the Role of Surface Traps in CdSe/CdS/ZnS Nanocrystal Photoluminescence Decay Dynamics. *Proc. Natl. Acad. Sci. U.S.A.* **2009**, *106*, 3011−3016.
(42) Marcus, R. A.; Sutin, N. Electron Transfers in Chemistry and Biology. *Biochim. Biophys. Acta* **1985**, *811*, 265−322.
(43) Lakowicz, J. R. *Principles of Fluorescence Spectroscopy*, 3rd ed.; Springer: New York, 2006.
(44) Wu, S.; Dzubiella, J.; Kaiser, J.; Drechsler, M.; Guo, X. H.; Ballauff, M.; Lu, Y. Thermosensitive Au-PNIPA Yolk-Shell Nanoparticles with Tunable Selectivity for Catalysis. *Angew. Chem., Int. Ed.* **2012**, *51*, 2229−2233.
(45) Debye, P. Reaction Rates in Ionic Solutions. *Trans. Electrochem. Soc.* **1942**, *82*, 265−272.
(46) Szleifer, I. Protein Adsorption on Surfaces with Grafted Polymers: A Theoretical Approach. *Biophys. J.* **1997**, *72*, 595−612.
(47) Scrimgeour, C. M.; Harwood, J. L. In *The Lipid Handbook with Cd-Rom*, 3rd ed.; Gunstone, F. D., Harwood, J. L., Dijkstra, A. J., Eds.; CRC Press: Boca Raton, FL, 2007.
(48) Tagliazucchi, M.; Tice, D. B.; Sweeney, C. M.; Morris-Cohen, A. J.; Weiss, E. A. Ligand-Controlled Rates of Photoinduced Electron Transfer in Hybrid CdSe Nanocrystal/Poly(Viologen) Films. *ACS Nano* **2011**, *5*, 9907−9917.